

Highlights

Mechanical softening and enhanced elasticity of lunar olivine probed via nanoindentation and high-pressure X-ray diffraction measurements

P. Grèbol-Tomàs, J. Ibáñez-Insa, J. M. Trigo-Rodríguez, E. Peña-Asensio, R. Oliva, D. Díaz-Anichtchenko, P. Botella, J. Sánchez-Martín, R. Turnbull, D. Errandonea, A. Liang, C. Popescu, J. Sort

- Lunar olivine in meteorite NWA12008 is softer and more elastic than terrestrial olivine, as revealed by nanoindentations.
- HP-XRD measurements show that the b orthorhombic axis of lunar olivine is more compressible than that of terrestrial olivine.
- Similar conclusions may apply to other extraterrestrial olivines, such as those in some ordinary chondrites.
- Space weathering could explain the observed mechanical softening, which might be partly related to structural changes at the chemical bond scale.

Mechanical softening and enhanced elasticity of lunar olivine probed via nanoindentation and high-pressure X-ray diffraction measurements

P. Grèbol-Tomàs^{a,b,*}, J. Ibáñez-Insa^{c,*}, J. M. Trigo-Rodríguez^{a,b}, E. Peña-Asensio^d, R. Oliva^c, D. Díaz-Anichtchenko^c, P. Botella^e, J. Sánchez-Martín^e, R. Turnbull^e, D. Errandonea^e, A. Liang^f, C. Popescu^g and J. Sort^{h,i}

^aInstitut de Ciències de l'Espai (ICE-CSIC), C/ Can Magrans, s/n, Cerdanyola del Vallès, 08193, Barcelona, Catalonia, Spain

^bInstitut d'Estudis Espacials de Catalunya (IEEC), C/ Esteve Tarradas 1, Parc Mediterrani de Tecnologia (PMT) Campus Baix Llobregat - UPC, Castelldefels, 08860, Barcelona, Catalonia, Spain

^cGeosciences Barcelona (GEO3BCN-CSIC), C/ Lluís Solé i Sabarís, s/n, Barcelona, 08028, Catalonia, Spain

^dDepartment of Aerospace Science and Technology, Politecnico di Milano, Via La Masa 34, Milano, 20156, Italy

^eDepartamento de Física Aplicada-ICMUV, MALTA Consolider Team, Universidad de Valencia, C/ Dr. Moliner 50, Burjassot, 46100, Valencia, Spain

^fCentre for Science at Extreme Conditions and School of Physics and Astronomy, University of Edinburgh, Edinburgh, EH9 3FD, Scotland, United Kingdom

^gCELLS-ALBA Synchrotron Light Facility, C/ de la Llum 2-26, Cerdanyola del Vallès, 08290, Barcelona, Catalonia, Spain

^hDepartament de Física, Universitat Autònoma de Barcelona (UAB), C/ dels Til·lers s/n, Cerdanyola del Vallès, 08193, Barcelona, Catalonia, Spain

ⁱInstitució Catalana de Recerca i Estudis Avançats (ICREA), Passeig Lluís Companys 23, Barcelona, 08010, Catalonia, Spain

ARTICLE INFO

Keywords:

Planetary materials
Lunar rocks
Chondrites
Mechanical properties
Elasticity
Nanoindentation
Diamond anvil cell

ABSTRACT

Mechanical properties of minerals in planetary materials are not only interesting from a fundamental point of view but also critical to the development of future space missions. Here we present nanoindentation experiments to evaluate the hardness and reduced elastic modulus of olivine, $(\text{Mg, Fe})_2\text{SiO}_4$, in meteorite NWA 12008, a lunar basalt. Our experiments suggest that the olivine grains in this lunaite are softer and more elastic than their terrestrial counterparts. This may be attributed to macroscopic effects, like increased porosity, or even to modifications at the chemical bond scale. We have performed high-pressure X-ray diffraction (HP-XRD) measurements to probe the elastic compressibility properties on this meteorite and, for comparison purposes, on three ordinary chondrites. The HP-XRD results suggest that the axial compressibility of the orthorhombic b lattice parameter of olivine is higher in NWA 12008 and also in the highly-shocked Chelyabinsk meteorite, relative to terrestrial olivine. The origin of the observed differences may be the consequence of a combination of factors reflecting their complex history. The combined study by nanoindentations and HP-XRD of the mechanical and elastic properties of meteorites and returned samples opens up a new avenue to characterize these materials that will be crucial for future extraterrestrial resource utilization purposes.

1. Introduction

The investigation of the mechanical properties of solids is essential to develop new materials with improved properties or to optimize the performance of existing applications. From a more fundamental perspective, understanding the mechanical and elastic properties of solids allows one to probe their atomic and molecular structure and also the relationship between microstructure (grain size, porosity, fracturing, or defects) and macroscopic behavior (performance, durability, or structural integrity).

In particular, the study of the mechanical properties of planetary materials is currently attracting considerable research interest. In this regard, there are ongoing research lines aiming to characterize the physico-chemical properties and the mechanical response of construction materials fabricated with lunar regolith simulants for the purpose of

the so-called in-situ resource utilization (ISRU; Pilehvar et al., 2020; Neves et al., 2020). Space agencies envisage the extraction of raw materials and minerals from planetary bodies, either asteroids, moons or planets, in order to build the infrastructures required by future dwellers (Lim et al., 2017; Naser, 2019; Duffard et al., 2021; Liu et al., 2024). The first investigations on the behavior of concrete made with lunar material date back to the 80s of the last century, which relied on samples returned by the Apollo 16 mission (Lin et al., 1988).

On the other hand, many of the current designed space missions involve contact processes that play a crucial role for their success. Examples of this kind are the recent landing and sample extraction on asteroids (101955) Bennu (OSIRIS-Rex mission; Lauretta et al., 2017), (25143) Itokawa (Hayabusa mission; Yano et al., 2006), or (162173) Ryugu (Hayabusa2 mission; Watanabe et al., 2019). Contact processes are also critical for the success of lunar missions like Chang'e 7 (Wang et al., 2023), Chandrayaan-3 (Durga Prasad et al., 2023) or the Artemis mission (NASA, 2020). For instance, as shown by Tardivel et al. (2014) for the case of contact motion on asteroidal surfaces, the contact dynamics

*Corresponding authors

✉ grebol@ice.csic.es (P. Grèbol-Tomàs); jibanez@geo3bcn.csic.es (J. Ibáñez-Insa)

ORCID(s): 0009-0004-2554-890X (P. Grèbol-Tomàs);

0000-0002-8909-6541 (J. Ibáñez-Insa); 0000-0002-9378-4048 (R. Oliva);

0000-0001-7912-0248 (R. Turnbull)

strongly depends on the coefficient of restitution which, in turn, is determined by the elastic properties of the two involved bodies.

Similarly, in the field of planetary defense, the amount of momentum transferred to a hazardous asteroid in a deflection mission is expected to be strongly dependent upon the mechanical properties of its surface, as observed in the recent DART mission (Cheng et al., 2023; Daly et al., 2023; Roth et al., 2023; Thomas et al., 2023; Raducan et al., 2024). In this sense, fragmentation modelling also requires proper knowledge of the micromechanical properties of the impacted object (Davison et al., 2016; Robin et al., 2024).

Among the wide range of methodologies and analysis techniques available, nanoindentation is arising as a promising tool to assess mechanical performance of extraterrestrial materials because it is a minimum-damaging test that can preserve invaluable samples. In nanoindentation, the sample is indented with a nanometer-sized sharp end. Mechanical properties of the sample at mineral scale are extracted from the amount of indentation displacement as a function of the applied load. However, mechanical properties of individual minerals do not strictly correspond to macroscopic whole-rock properties. These can ultimately be recovered with appropriate modeling and careful characterization of fractures, as shown for the case of granite samples (Xu et al., 2023) and even in meteorites (Tang et al., 2023).

Nanoindentation has been reported used to investigate natural and industrial materials (Tabor, 2000; Ma et al., 2020), but also to characterize extraterrestrial soil simulants, including lunar (Gholami et al., 2022). To a lesser extent, it has also been applied to analyze natural extraterrestrial samples. The first works dealing with nanoindentation measurements showed that valuable information can be gained with this technique. Tang et al. (2023) attempted to model the mechanical properties of asteroid rocks based on the results of nanoindentation experiments on meteorites. Moreover, this technique has already been used to study a number of meteorites from different parent bodies (e.g. ordinary and carbonaceous chondrites; Yomogida and Matsui, 1983; Horii et al., 1990; Moyano-Camero et al., 2017; Peña-Asensio et al., 2024), returned samples from Itokawa (Tanbakouei et al., 2019) and Bennu (Hoover et al., 2024) asteroids, and also returned lunar rocks (Nie et al., 2023).

In particular, nanoindentation tests were recently performed by Peña-Asensio et al. (2024) in order to probe the mechanical properties of different minerals in a series of lunar meteorites. The findings of these authors suggested that, in some lunaite, the hardness (H) and the reduced elastic modulus (E_r) of the widely studied olivine mineral might be slightly lower than in terrestrial olivine. This finding would be highly relevant, as it would indicate that lunar and terrestrial materials might exhibit different mechanical behavior. However, the differences observed in that work were not sufficiently conclusive due to limited statistical robustness.

In this work we have identified a lunaite, the NWA 12208 meteorite, which contains olivine grains with H and E_r

values that are significantly lower than those measured in terrestrial olivine. The aim of the present work is to evaluate the mechanical properties of lunar olivine in this meteorite and compare the results with those measured on terrestrial olivines. Here we have focused our attention on olivine because the mechanical properties of this mineral have been widely studied in the past due to their relevance for the geodynamics of the lithosphere and the Earth's mantle (Kranjc et al., 2016, 2020; Baral et al., 2021; Badt and Goldsby, 2023; Kumamoto et al., 2024), and for being one of the most common minerals in extraterrestrial objects (e.g. Rubin and Ma, 2017). Moreover, similar investigations on other major minerals in lunar rocks would have been more involved due to compositional or structural complexity (e.g. the strong variability of stoichiometry in Fe/Ti/Mg oxides, or cationic substitutions in pyroxenes).

Given that NWA 12208 is found to exhibit clearly reduced H and E_r values, we have performed additional high-pressure X-ray diffraction experiments (HP-XRD) in order to obtain an independent measurement of the elastic properties of olivine in this meteorite. Although HP-XRD was used in the past to investigate phase transitions of some meteorite minerals (Chandra et al., 2013; Chandra et al., 2016), a comprehensive study of the pressure behavior of minerals in meteorites, and particularly in lunaite, is still lacking. This type of study is particularly complex because of the multiphase nature of the samples.

The HP-XRD experiments allowed us to determine the bulk modulus of olivine in the lunaite, which we showed is comparable, within experimental error, to that in terrestrial olivine and also to three different ordinary chondrites. In contrast, our HP-XRD results suggest that the b lattice parameter of olivine in NWA 12008 is more compressible than in terrestrial olivine. Other ordinary chondrites might show a similar behavior.

This article is organized as follows: in Section 2 we describe the analyzed samples and the different techniques used for its characterization; the results are presented and discussed in Section 3; and, finally, the main conclusions of this work can be found in Section 4.

2. Sample description and methodology

NWA 12008 is a highly-shocked lunar mare basalt with a rich mineralogy that is the consequence of its igneous history. Pyroxene and olivine are the main minerals in this achondrite, as confirmed by laboratory XRD measurements on powdered material (not shown). These phases can be identified as a clinoenstatite mineral and Fe-rich forsterite, respectively. As reported in the Meteoritical Bulletin¹, NWA 12008 also features sizable amounts of plagioclase and ilmenite, which are not detected by XRD. Other minerals such as barite or troilite have also been reported to be contained in NWA 12008 (Gattacceca et al., 2020).

¹<https://www.lpi.usra.edu/meteor/metbull.php>



Figure 1: Mosaic of the NWA 12008 lunar meteorite sample under reflected light. Each grid separator corresponds to 2 mm in physical scale.

A thin section of NWA 12008 was prepared, and a Zeiss Scope A1 microscope was used to build its mosaic under reflected light (Figure 1). The mosaic in Figure 1 includes a grid with 2-mm² square regions of interest (ROIs) that are conveniently labeled for proper identification of the studied areas. The high degree of fracture of this meteorite is clearly seen in all regions of the sample (see Figure 1). The most apparent feature is the large crack going across the bottom part of the image. Pyroxenes and olivines appear as submillimetric homogeneous regions, while the whitish, highly reflective minerals correspond to the opaque minerals in the sample (MacKenzie and Adams, 1994).

2.1. Characterization using nanoindentation

A summary of the analytical procedure employed in this work is displayed in Figure 2. As nanoindentations allow retrieving the mechanical properties locally, at a submicron scale, one must carefully select the region to be nanoindented. Thus, we first conducted a visual inspection of the sample under the petrographic microscope. This allowed us to obtain a preliminar identification of the major minerals and, in particular, to identify the largest, most homogeneous olivine grains to perform the nanoindentations. For instance, the rhomboid-shaped mineral grain at the bottom right region of Figure 2 (Step 1) was identified as an olivine grain. This grain belongs to the J10 ROI in Figure 1. It should be noted that the thickness of the thin section is not the standard 30 μm, and therefore the interference colors are not the usual ones.

The selected olivine regions were nanoindented by using an Anton-Paar nanoindenter (NHT2 model). We used a diamond pyramidal-shaped with triangle-based tip, also known as Berkovich, to perform the experiments. The nanoindenter tip was calibrated using a fused silica sample (Fischer-Cripps and Nicholson, 2004). All indentation tests comprised a loading segment to 100 mN at a 200 mN/min, followed by a steady pause of 2 s. Unloading was performed at the same rate. These parameters were chosen not to exceed the

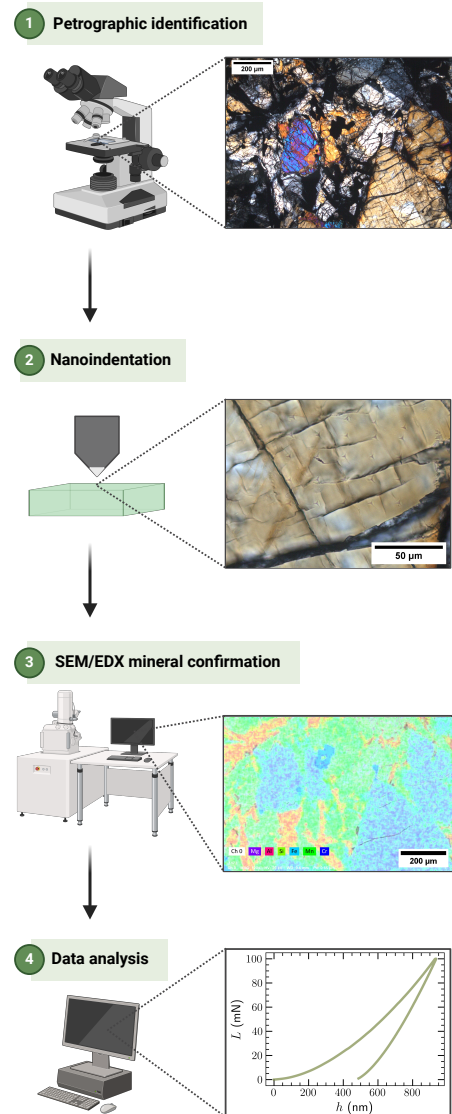


Figure 2: Methodology scheme, with images taken from NWA 12008 lunar meteorite. In this illustration, all images from Steps 1 to 3 are taken from the delimiting region between quadrants I-J 10 in Figure 1. Petrographic images (Steps 1 and 2) were taken under cross-polarized light (interference colors are not standard because the thin section is not exactly 30 μm thick). The image for Step 2 shows the NWA 12008 high olivine relief and a 5 × 5 nanoindentation matrix of the rhomboid-shaped mineral seen in Step 1. Elemental analysis of the same region was conducted by SEM/EDX mapping (Step 3). Each elemental abundance is represented by different color intensities: purple for Mg, red for Al, green for Si and Mn, light blue for Fe and dark blue for Cr. Step 4 includes an example of an applied force (L) vs displacement curve (h) from a nanoindentation in Step 3. Created in <https://BioRender.com>.

maximum load that the studied minerals can support. As seen in Figure 2 (Step 2), microscale triangular marks were the only remnant of the nanoindentations.

Even though nanoindentation is a powerful technique to characterize the mechanical properties of a sample, one of its main drawbacks is that the results may depend on the

maximum applied load and the surface roughness of the material (Ayatollahi et al., 2020). In order to control for these effects, we also nanoindented a sample containing terrestrial olivine with the same loading and unloading parameters as those used for the NWA 12008 olivines.

2.1.1. Mineral confirmation using SEM-EDX

In order to fully characterize the composition of the nanoindented regions and confirm that these did correspond to olivine minerals, we conducted EDX microanalyses by using a Hitachi TM4000plus tabletop SEM equipped with a Bruker EDX detector. With this technique we assured an objective mineral identification, rather than relying only on the petrographic microscope analysis. We mapped the abundance of the main elements in the field of view (Step 3 in Figure 2) and characterized the relative abundances in the investigated areas. The relative atomic abundances between Fe, Mg, and Si allowed us to confirm that all the nanoindented regions considered in this work correspond to olivine. From the ratio between Mg and Fe atomic abundances (not given), we obtained the forsterite/fayalite content of the studied olivines.

2.1.2. Nanoindentation parametrization

A usual nanoindentation plot shows the amount of displacement of the nanoindenter (h) versus the applied loading force to the surface (L). A typical h - L curve is represented in Figure 2 (Step 4). Due to the material plasticity, the loading and unloading curves do not follow the same path. The whole curve can be parametrized to extract the hardness (H) and reduced elastic modulus (E_r) at the nanoindented spot, using the method described in Oliver and Pharr (2011).

As is well known, H is the mechanical property characterizing the material resistance to permanent deformation after application of a load. It can be calculated at the point of maximum load (L_{max}) using the projected contact area A_c on the horizontal plane as

$$H = \frac{L_{max}}{A_c}. \quad (1)$$

For an ideal Berkovich nanoindenter, the contact area is $A_c = 24.5h_c^2$, where h_c is the contact depth of the tip.

On the other hand, the Oliver-Pharr method allows calculating E_r , which is directly related to the material stiffness, S , which, in turn, is given by the slope of the load-displacement curve (Step 4 plot in Figure 2) as

$$S = \frac{dL}{dh} = 2\beta \sqrt{\frac{A_c}{\pi}} E_r, \quad (2)$$

where $\beta = 1.034$ is a constant related to the geometry of the Berkovich indenter (Fischer-Cripps and Nicholson, 2004).

The reduced elastic modulus characterizes the elastic deformation of the material under an applied force. This parameter is directly measured by the nanoindenter and includes the contributions to the measured stiffness of both the nanoindenter tip (diamond) and the material surface. The reduced elastic modulus can be related to Young's modulus

of the measured sample with further parametrization (Oliver and Pharr, 1992).

The areas below the loading and unloading curves correspond to the total (W_T) and plastic (W_{el}) works during the indentation process, respectively. The plastic energy involved in the process can be found as $W_{pl} = W_T - W_{el}$. These values provide insights on the recovery stage, back to the initial state after the nanoindentation, i.e. on the reversible and irreversible energies exchanged during the process (Fischer-Cripps and Nicholson, 2004; Jha et al., 2012; Liu et al., 2016). In this work, we used the plastic and elastic works as complementary parameters to identify samples near to cracks or grain boundaries (Section 3.1).

2.2. HP-XRD

Room-temperature powder angle-dispersive XRD measurements were performed on different meteorite samples as a function of hydrostatic pressure. All samples were carefully powdered and loaded with a 4:1 methanol-ethanol mixture in a membrane-type diamond anvil cell (DAC) with diamond culets of 400 μm in diameter. The measurements were performed during the upstroke and below 12 GPa, since the methanol-ethanol pressure transmitting medium exhibits an abrupt reduction of hydrostaticity above this pressure value.

The HP-XRD experiments were performed in the BL04-MSPD beamline at ALBA synchrotron, Cerdanyola del Valès, Barcelona (Fauth et al., 2013). This beamline is equipped with Kirkpatrick-Baez mirrors, which allow focusing the monochromatic beam (wavelength of 0.4246 Å, corresponding to the absorption K-edge of Sn), and a Rayonix CCD detector with an active area of 165-mm diameter.

The samples included in the HP-XRD study consisted of the NWA12008 meteorite together with 3 additional ordinary chondrites, which served us to evaluate the compression behavior in other non-terrestrial materials: Aiguile (classified as H5), Chelyabinsk (LL5), and Viñales (L6). The pressure applied on the samples was determined with the equation of state (EoS) of copper (Dewaele et al., 2004). The associated error to the pressure determination, including the pressure gradients inside the DAC, is lower than 0.2 GPa. The sample-to-detector distance, along with various detector geometrical parameters of the experiment, were calibrated with the DIOPTAS software (Prescher and Prakapenka, 2015). For this purpose, diffraction data from LaB₆ was used.

In order to obtain enough XRD signal from reflections of the mineral olivine in the studied samples, many different XRD measurements were performed at each applied pressure. This was achieved by mapping the sample cavity. For the subsequent analysis of the data, only the best scans were employed. This was particularly important in the case of NWA 12008, since the overall olivine content of this meteorite is much lower than that of the ordinary chondrites.

Structural analyses for the olivine mineral contained in the studied samples were performed with the program TOPAS 4.2 from Bruker. Most of the analyses relied on a

full-pattern matching based on the Pawley method, which allowed us to obtain the unit-cell parameters of olivine as a function of hydrostatic pressure. Equations of state (EoS) were fitted to the pressure-volume or pressure-lattice parameter data by using EosFit-GUI (Gonzalez-Platas et al., 2016), which allowed us to extract the compressibility properties of olivine in the investigated samples.

3. Results and discussion

Olivine, $(\text{Mg,Fe})_2\text{SiO}_4$, is one of the most common minerals in the Solar System. It is a solid solution between forsterite (Fo), Mg_2SiO_4 , and fayalite (Fa), Fe_2SiO_4 . Olivine is one of the main minerals in the Earth's mantle and has been widely studied in the past due to its relevance in geodynamics (e.g. Mackwell et al., 1990; Peslier et al., 2010). In other planetary bodies, such as Venus or Mars, olivine has been found to be a major component of their mantles (Morgan and Anders, 1980; Fegley, 2003; Taylor and Scott, 2003; Ronco et al., 2015). Smaller bodies such as chondrite meteorites also contain olivine (Rubin and Ma, 2017, and references therein). In fact, olivine is the main mineral in interstellar dust particles, formed during the last stages of stellar evolution (Jones, 2000; Min, M. et al., 2007). In the present work, we use nanoindentations and HP-XRD measurements to investigate the mechanical and elastic properties of olivine in samples from different origins.

3.1. Nanoindentation results

A total of 78 nanoindentations on lunar olivine grains were performed in 5 different ROIs of the NWA 12008 thin section. Due to the high degree of fracture of the sample, some nanoindentations were conducted too close to visible microfractures or grain boundaries, which are not representative of the whole mineral (Avadanii et al., 2023). In particular, three of the measurements were found to be clearly deviated from the general behavior (including H , E_r , W_{el} , and W_{pl} parameters) and were discarded.

In turn, 91 nanoindentation measurements were performed on terrestrial olivine. The selected sample showed grains with uniform chemical composition and no micrometric fractures, contrary to the case of NWA 12008. Therefore, no outlier removal was required.

Figure 3 shows the measured values from the individual nanoindentations on NWA 12008 and terrestrial olivines in a H vs. E_r plot. The histograms on the top and right sides of the figure show the distribution of H and E_r values obtained for NWA12008 (dashed lines) and for terrestrial olivine (dotted lines). As can be seen in the figure, most NWA 12008 olivine data points (solid dots) exhibit significantly lower hardness and reduced elastic modulus compared with their terrestrial counterparts (open dots), which cluster around $H \sim 13$ GPa and $E_r \sim 160$ GPa. These values are in good agreement with those reported in the literature for terrestrial olivine (Kranjc et al., 2016). Clearly, the data points from NWA 12008 tend to populate an area with significantly lower H and E_r values, thus suggesting that the lunar olivine in this meteorite is softer and more elastic. Table 1 shows

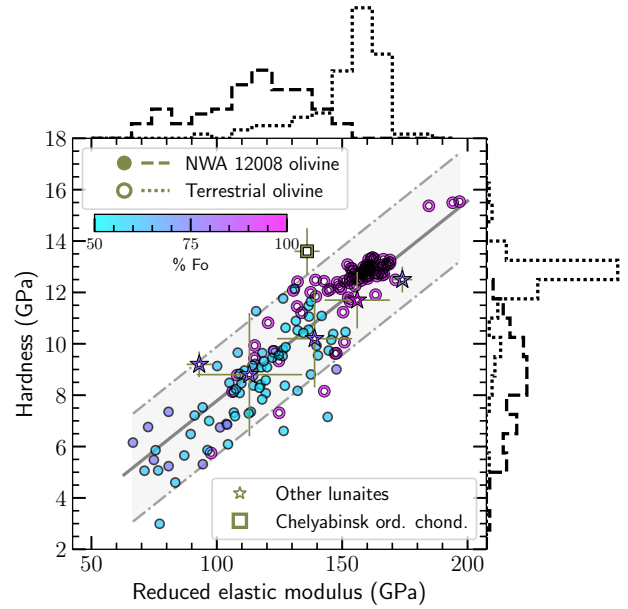


Figure 3: Values of hardness and reduced elastic modulus for each individual nanoindentation in this work. Closed circles correspond to NWA 12008 lunar olivine data, while open circles correspond to terrestrial olivine values. The solid line corresponds to the all-data linear fit. The region delimited with dash-dotted lines represents the 95% prediction interval of the data. The marginal histograms show the density distribution of terrestrial and NWA 12008 values along the hardness and reduced elastic modulus spaces. Values from olivines in other lunar meteorites (stars, Peña-Asensio et al., 2024) are also shown, as well as those from the Chelyabinsk meteorite (square, Moyano-Cambero et al., 2017), along with their reported errors. Each dot is colored according to the percentage of forsterite (% Fo) in the olivine except for the Chelyabinsk meteorite, for which no % Fo was reported.

Table 1

Mean values for hardness (H) and reduced elastic modulus (E_r) for NWA 12008 and terrestrial olivines. Experiments were conducted with a Berkovich tip with at 200 mN/min load rate, reaching a maximum load of 100 mN followed a steady pause of 2 s. Uncertainties correspond to 1σ standard deviation of the measurements.

	H (GPa)	E_r (GPa)
NWA 12008 olivine	8.4 ± 1.9	114 ± 21
Terrestrial olivine	12.2 ± 1.6	153 ± 17

a compilation with the mean values of H and E_r for the lunar (NWA 12008) and terrestrial olivines measured in this work. The errors reported in the table represent the standard deviation of the mean values.

Figure 3 also shows H and E_r values in olivine grains of other extraterrestrial sources, as reported in Moyano-Cambero et al. (2017); Peña-Asensio et al. (2024). The plot also includes the 95% prediction interval for all the measured data (lunar and terrestrial), which displays a linear trend with a H/E_r ratio equal to 0.0778 ± 0.0030 . This value is only

slightly lower than that reported in Kranjc et al. (2016) for terrestrial olivine (0.0790 ± 0.0040). The hardness of the Chelyabinsk olivine is of the order of the terrestrial values, while its reduced elastic modulus is slightly lower than that from terrestrial olivine. On the other hand, all the H and E_r values for the lunaites studied in Peña-Asensio et al. (2024) lie within the 95% prediction interval of the linear regression. Although the measurements of Peña-Asensio et al. (2024) employed slightly different nanoindentation parameters, the data points from the lunaites studied in that work match well with the present data on NWA 12008. Their work did not provide concluding evidence for softening, as that found here for NWA 12008, due to limited statistics.

The distribution of H and E_r values in NWA 12008 olivine shown in Figure 3 is significantly more scattered compared to that measured in the terrestrial sample. We attribute this observation to relatively large differences in the particular environment of the minerals within the meteorite slab (Angel et al., 2014, 2015; Mazzucchelli et al., 2019). Nevertheless, the overall H and E_r values measured for the olivine grains in NWA 12008 and also in other lunaites (see Peña-Asensio et al. (2024) for details) are clearly lower than in its terrestrial counterparts.

It is important to remark that the fact that lunar olivines have lower H and E_r than their terrestrial counterparts does not seem to be a consequence, at least solely, of the particular Mg/Fe (Fo/Fa) composition of the nanoindented olivine grains. The color scale in Figure 3 serves to represent the molar content of Fo in the analyzed olivines. The measured lunar olivines cover a Fo range between 55% and 75%, which is lower than the forsterite content in the analyzed terrestrial sample (Fo = 89%). At first glance, one might conclude that this might explain why terrestrial olivine is harder and less elastic than lunar olivine. However, it is worth mentioning that the mechanical properties of the lunaite olivines do not seem to exhibit any monotonic behavior as a function of Fo. In fact, olivines in the lunar sample seem to even show decreasing H and E_r values with increasing forsterite content. For instance, numerous olivine grains of NWA 12008 with Fo \sim 75% show much lower H and E_r values than other grains with larger Mg contents. The fact that many data points from lunar olivine populate a region below $H = 8$ GPa and $E_r = 100$ GPa cannot be solely explained by a compositional effect.

To further support this conclusion, we note that the Vickers hardness (H_V) and the shear stress modulus (G) of polycrystalline materials exhibit a universal trend, as discussed in Chen et al. (2011). For the present work, and given the similarities and comparable H values extracted with Vickers and Berkovich experiments (Chudoba et al., 2006), it can be assumed that the data of Chen et al. (2011) can be extrapolated to the present case. As shown in that work, H_V and G in intrinsically-brittle materials can be assumed to be linear, with $H_V = 0.151G$. Using this expression together with data from Bass (1995), where the shear stress of pure forsterite and fayalite in terrestrial olivine was characterized, it is possible to evaluate the expected H values for olivines

with Fo \sim 50%, i.e., for the lowest Mg contents measured in NWA 12008 olivines. These authors found that pure forsterite has $G = 81.1$ GPa, while $G = 50.7$ GPa in pure fayalite. As a rough approximation, we can consider that the shear stress for a 50% Fo olivine is \sim 66 GPa. According to the relation between H_V and G given in Chen et al. (2011), using the H values that we measure in terrestrial olivine, this would correspond to a hardness of 9.9 GPa for Fo = 50%. This value is still much larger than the H values measured in the lunaites, where much lower values are most frequently found (Figure 3). The present estimation of H based on the data of Chen et al. (2011) supports the idea that the differences between lunar and terrestrial olivines cannot be solely attributed to compositional effects.

Figure 4 shows average H and E_r values obtained in this work for lunar and terrestrial olivines. For comparison, values from different types of terrestrial olivines (single crystal, polycrystalline and amorphous) reported in the literature (Kranjc et al., 2016; Baral et al., 2021) are also plotted in the figure, together with data for the Chelyabinsk meteorite (Moyano-Camero et al., 2017). The error bars indicate the standard deviation for each collection of measurements. Note that different nanoindentation parameters were used in different works. Therefore, some caution should be taken when comparing the corresponding data. In any case, as can be clearly seen in Figure 4, lunar olivines in NWA 12008 are significantly softer and more elastic than the rest of (poly)crystalline olivines (Kranjc et al., 2016), including those in the highly-shocked Chelyabinsk chondrite. Error bars for NWA 12008 do not overlap with the rest of crystalline olivine samples. Interestingly, amorphous olivine (Baral et al., 2021) was found to exhibit much lower hardness values, comparable to those measured in NWA 12008.

The reason of the softening of NWA 12008 and other lunaites is still an open question and could be attributed to many different phenomena, ranging from lattice disorder to the presence of (sub)micrometric features like microfractures or increased porosity. Any of these might have been caused by alterations due to shock compaction and fracturing produced by collisional processing, a key process in space weathering. For instance, Jiang et al. (2024) found that H and E_r in olivine are reduced with increasing density of atomic hydrogen in the lattice (simulating a solar wind effect). The fact that amorphous olivine is much softer than the (poly)crystalline mineral suggests that lattice disorder might have a bearing on the mechanical properties of olivine. Such disorder might include defects in various dimensions including point, line and planar defects and even 3D inclusions (Demouchy, 2021). The latter would have been introduced in the original lunar magmas.

With regard to the possible effect of microfractures on the mechanical behavior of olivine, it is interesting to compare the H and E_r values for olivine in the lunaites with those measured in the Chelyabinsk meteorite (Figure 4). This ordinary chondrite is highly shocked and contains a large number of microfractures and even darkened areas (Moyano-Camero et al., 2017). However, the measured H

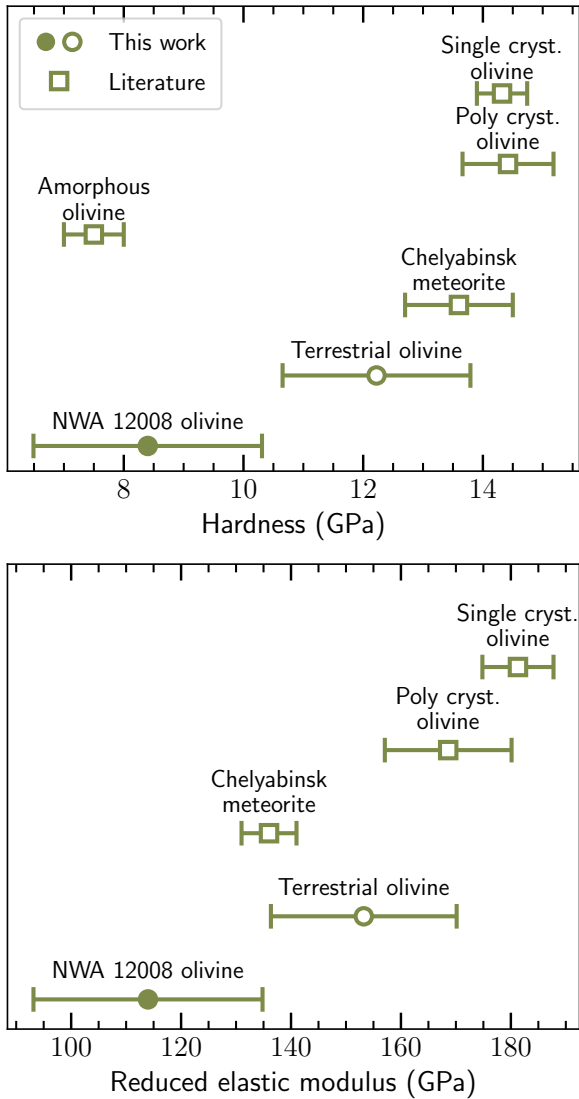


Figure 4: Mean measured values of olivine hardness and reduced elastic modulus in different sources. Markers distinguish literature values from those values extracted from nanoindentations of this work. As in Figure 3, closed circles represent the NWA 12008 lunar olivine values, while open circles correspond to terrestrial olivine mean values. Single crystal and polycrystal olivine values are extracted from Kranjc et al. (2016), while the amorphous olivine values are taken from Baral et al. (2021). Chelyabinsk meteorite nanoindentation values are from Moyano-Camero et al. (2017). Error bars correspond to 1σ standard deviation.

and E_r values in NWA 12008 are still much lower than those in Chelyabinsk, the mechanical behavior of which is not far from terrestrial (poly)crystalline olivine. This result seems to indicate that shock-induced microfractures are not the main responsible for the softening observed in NWA 12008.

In relation to porosity, it is well known that, in many different types of materials, it can strongly affect H and, specially, E_r (e.g. Ramakrishnan and Arunachalam, 1993; Brantley and Mellott, 2000; Biener et al., 2004; Pellicer

et al., 2012; Tolu et al., 2013; Tanbakouei et al., 2019; Cariou et al., 2008; Magoaric and Danescu, 2009). In general, it is found that porosity implies morphological variations and/or an overall densification that may modify the mechanical behavior of materials at the submicron scale. Thus, it can be hypothesized that some lunar olivines may exhibit reduced H and E_r values due to increased porosity. With regard to this, Macke et al. (2010, 2011) measured the porosity of a large number of chondrites and achondrites. For the particular case of lunaites (4 samples included in their study), these authors found highly scattered porosity values, but in most cases comparable to those of ordinary chondrites (Macke et al., 2011). However, since no porosity data is available on NWA 12008, it is not possible to conclude whether the softening observed in this meteorite is a consequence of its high porosity. More work should be performed in different types of olivine-containing meteorites, and in particular in highly-porous achondrites like howardites (Macke et al., 2011), in order to ascertain the effect of porosity in the nanoindentation behavior of the olivine grains.

3.2. HP-XRD measurements

In the previous section, we have found strong evidence for reduced values of H and E_r in olivine grains of NWA 12008. The nanoindentation experiments have allowed us to obtain information about the elastic properties of lunar and terrestrial olivines and, in particular, of the reduced Young's modulus E_r , through the stiffness measurement of the contact between the tip and the studied material. The nanoindentation measurements involve, for all practical purposes, a macroscopic scale and a quasi-static regime.

In turn, HP-XRD measurements allow one to probe the compressibility of crystalline materials at the chemical bond scale through the determination of the unit-cell parameters as a function of pressure. By fitting the resulting pressure-volume EoS, parameters like the isothermal bulk modulus of the investigated material can be obtained. The bulk modulus, defined as $B_0 = -VdP/dV$, where P is pressure and V is volume, can be understood as the resistance of a substance to bulk compression and is related to other elastic properties such as Young's modulus.

In this section, we present synchrotron-based HP-XRD measurements to determine B_0 of olivine in NWA 12008 and compare the resulting value with that of terrestrial olivines. For comparison purposes, we have also performed HP-XRD measurements on three different ordinary chondrites.

Figure 5 shows selected powder XRD scans obtained for NWA 12008 at different pressure values. The expected shift of all the observed reflections to high 2θ values (i.e. to low lattice spacings) with increasing pressure is clearly seen. From the point of view of HP-XRD experiments, these are standard results and, qualitatively, they are very similar to those widely reported in the literature for terrestrial olivine by means of single-crystal XRD (sc-XRD) and powder XRD (Nestola et al., 2011, and references therein). In the case of the rest of ordinary chondrites included in the present study (scans not shown), similar results were obtained. In

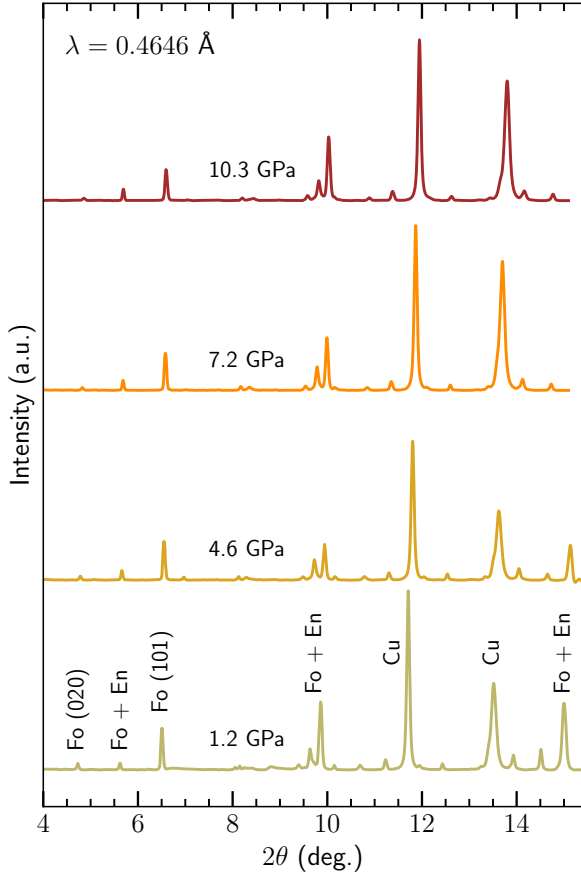


Figure 5: HP-XRD scans of lunaite NWA 122008 at different pressures. Selected reflections of forsterite (Fo) and clinoenstatite (En) are labelled in the lower scan. Peaks from copper are also indicated.

fact, the particular compression behavior of different types of samples (terrestrial, lunar, and asteroidal) with similar mineralogy only emerges after a careful analysis of the experimental data.

The Pawley method was used to extract the orthorhombic unit-cell parameters of olivine as a function of pressure for the different meteorites measured by HP-XRD. The upper panel of Figure 6 shows the resulting unit-cell volume, as a function of pressure, for the particular case of NWA 12008. Data up to 9.5 GPa is shown in the figure, together with a fit using a third-order isothermal Birch-Murnaghan EoS (BM-3):

$$P(V) = \frac{3B_0}{2} \left[\left(\frac{V_0}{V} \right)^{7/3} - \left(\frac{V_0}{V} \right)^{5/3} \right] \cdot \left\{ 1 + \frac{3}{4}(B' - 4) \left[\left(\frac{V_0}{V} \right)^{2/3} - 1 \right] \right\}, \quad (3)$$

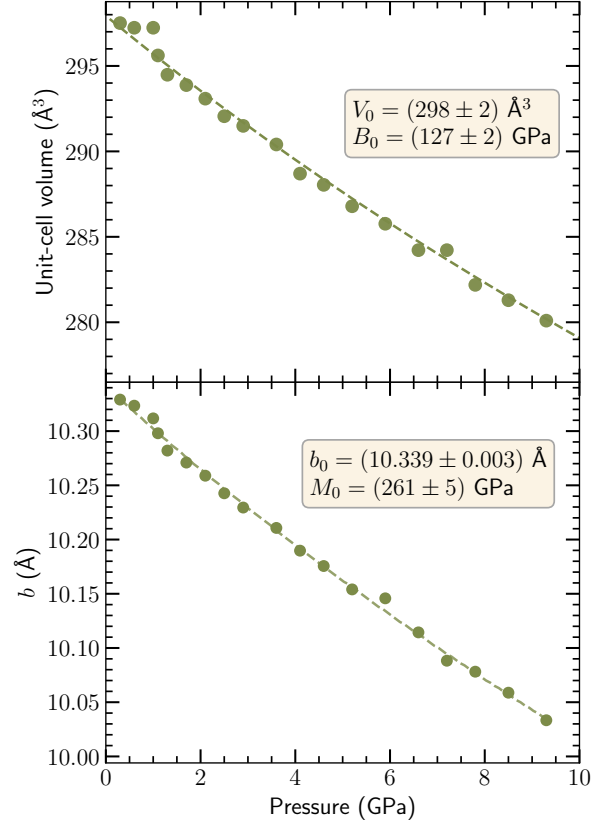


Figure 6: Upper panel: pressure-volume dependence (solid dots) as obtained from HP-XRD measurements for lunaite NWA 12008. The curve shows the result of a fit to the experimental data with a third-order Birch-Murnaghan equation of state. Lower panel: pressure dependence of the b lattice parameter of olivine (solid dots) as extracted from the evolution of the (020) reflection. The curve shows the result of a fit to the experimental data with a second-order Birch-Murnaghan equation of state.

where V_0 , B_0 and B' are, respectively, the zero-pressure unit-cell volume, the zero-pressure bulk modulus and its pressure derivative. Normalized pressure-eulerian strain plots (not shown) indicated that B' is close to 4, thus suggesting that a second-order BM EoS (BM-2, where $B' = 4$ in Equation 3) might suffice for the EoS fits. However, as previous works that obtained accurate EoS parameters for olivines with sc-XRD measurements relied on BM-3 (Nestola et al., 2011), here we employ this EoS to fit our HP-XRD data. For this purpose, the well-known correlation between the fitted B_0 and B' parameters for BM-3 EoS (Angel, 2000) needs to be considered. This correlation typically leads to large uncertainties in the fitted values. To avoid this problem, we fixed B' to the expression $B' = 31.104 - 0.0874V_0$, which was obtained by adjusting the $B'-V_0$ dependence reported in Nestola et al. (2011) to a linear equation. As shown in that work, B_0 and V_0 in the terrestrial olivines increases with Fe content, while B' tends to slightly decrease.

Figure 7 shows a compilation of the V_0 and B_0 values extracted with BM-3 fits (fixing B' as explained above),

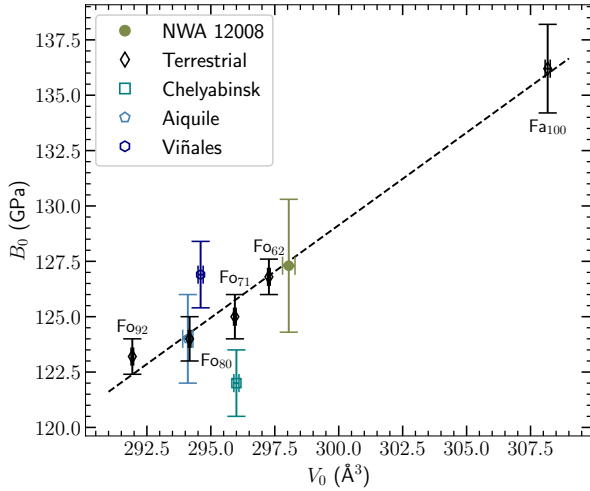


Figure 7: Bulk modulus (B_0) versus zero-pressure volume (V_0) for olivine in the different samples measured in this work by HP-XRD. The B_0 and V_0 values were obtained by fitting the experimental pressure-volume data of Figure 6 (upper panel) with a third-order Birch Murnaghan EoS. Data for terrestrial olivines is taken from Nestola et al. (2011) and Zhang (1998) and their respective %Fo is labeled accordingly.

for the different meteorite samples included in the present HP-XRD study. For comparison purposes, the B_0 values reported in (Nestola et al., 2011) are also shown. A sc-XRD data point for a fayalite sample (Zhang, 1998) has also been included in the plot. It is important to remark that all these sc-XRD data for the (terrestrial) forsterite-fayalite solid solution were obtained below ~ 10 GPa, i.e., in a pressure range comparable to that of the present powder HP-XRD measurements.

Among the ordinary chondrites, only the Chelyabinsk meteorite seems to exhibit increased compressibility (i.e. reduced B_0) relative to the terrestrial samples, which would indicate that the decreased E_r values measured in this highly shocked meteorite by nanoindentation (see Figure 4 and Moyano-Cambero et al. (2017)) might be linked to changes at the chemical bond scale like, for instance, lattice disorder induced by shock metamorphism or cosmic-ray (proton) bombardment (Jiang et al., 2024).

In contrast, the bulk modulus obtained for olivine in NWA 12008 is comparable, within experimental error, to that measured in terrestrial olivines of similar Mg content (Figure 7). In this case, the HP-XRD experiments seem to indicate that the softening observed with nanoindentation experiments cannot be linked to structural changes at the crystal lattice level.

However, the previous analysis of the XRD scans with the Pawley method is strongly limited by the multiphase nature of the meteorite samples, as shown in Figure 5 for NWA 12008. In the particular case of this sample, the total olivine content is relatively low, and most of the reflections from olivine are overlapped to peaks from the pyroxene phase, the major mineral in this meteorite. As can be seen

in Figure 5, only the (020) and (101) reflections of olivine are not interfered by peaks from the pyroxene phase. Unfortunately, these two peaks alone do not allow extracting the pressure behavior of the three orthorhombic lattice parameters of olivine (a , b , and c).

To overcome this problem, we have performed an alternative analysis of the powder HP-XRD scans in which we have solely focused on the evolution of the (020) reflection of olivine, as this peak does not overlap with any other reflections and provides direct information about the compression behavior of the b parameter. Interestingly, this lattice parameter corresponds to the most compressible axis of olivine (Nestola et al., 2011) and, therefore, it may be more sensitive to structural changes of the crystal lattice of this mineral.

The bottom panel of Figure 6 shows the pressure behavior of b of olivine in NWA 12008 as determined from the evolution upon compression of the (020) reflection of this mineral. For simplicity, we extracted the axial bulk modulus of b , $M_0 = -bdP/db$, by fitting the data to a second-order Birch-Murnaghan EoS, which amounts to fixing the derivative of M_0 to 12. For this sample, we obtain a value $M_0 = (261 \pm 5)$ GPa, which is much lower than that reported in Nestola et al. (2011) for all the olivine samples studied in that work, up to Fa = 38% ($M_0 \equiv 3B_0b_0 = 279\text{--}282$ GPa).

Note, however, that the data of Nestola et al. (2011) were obtained with a BM-3 EoS. In this case, no compositional trend was found for the pressure derivative of M_0 . In order to properly compare between the M_0 values reported in that work and those of the present study, we have repeated the fits to the data of Nestola et al. (2011) by using a BM-2 EoS. Figure 8 shows the resulting EoS parameters for the olivine samples of that work, together with the results that we find for our meteorite samples. A data point for fayalite from Zhang (1998), also fitted with a BM-2 EoS, is included in the plot.

As can be seen in Figure 8, the M_0 values for the b axis in the terrestrial olivines decrease with increasing fayalite content. This is a well-known result in the case of terrestrial, high-quality olivines (Zhang, 1998; Nestola et al., 2011): while the a and c parameters of olivine become less compressible with increasing Fa, the b parameter becomes more compressible. Overall, the forsterite-fayalite solid solution becomes less compressible with increasing Fe content, as shown in Figure 7.

In the case of the meteorite samples studied in this work, within the experimental error of the present measurements and analyses, the b axis of olivine in several of the samples seems to be more compressible than expected for their particular composition. In the case of NWA 12008, there seems to be a significant reduction of the M_0 value, even after refitting the data of Nestola et al. (2011) to a BM-2 EoS (note that even larger differences would be seen without the BM-2 refitting). In the case of the Chelyabinsk meteorite, the resulting M_0 value also seems to be lower, in agreement with the behavior already observed for B_0 (Figure 7). In the case of Viñales, a reduced M_0 value for the b parameter is also

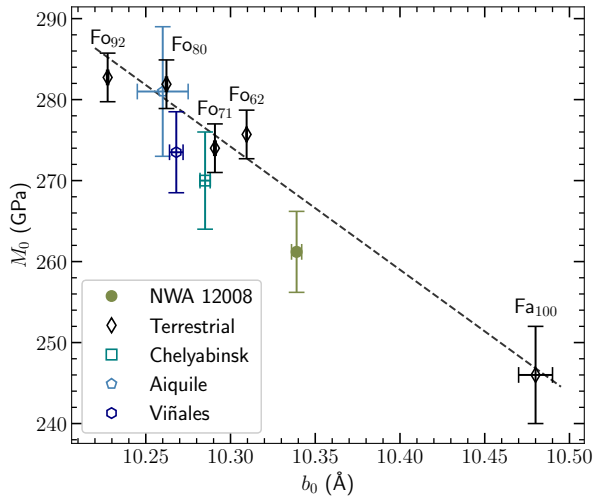


Figure 8: Bulk modulus for the orthorhombic b lattice parameter of olivine (M_0) versus the zero-pressure lattice-parameter value (b_0) for the different samples measured in this work by HP-XRD. The M_0 and b_0 values were obtained by fitting the experimental pressure-lattice parameter results plotted in the lower panel of Figure 6 with a second-order Birch Murnaghan EoS. Data for terrestrial olivines is taken from Nestola et al. (2011) and Zhang (1998) and their respective %Fo is labelled accordingly.

found. However, no nanoindentations are available for this meteorite. All these results for the axial compressibility of the b parameter of olivine in NWA 12008 and Chelyabinsk, in combination with the nanoindentation data available for these two meteorites, would indicate that the elastic properties in some planetary materials might be affected by some of the processes suffered along their complex history. For example, shock metamorphism or even cosmic-ray (proton) bombardment might have affected the crystalline quality of some of the mineral constituents, giving rise to elastic/mechanical softening. This would be particularly relevant for ISRU applications, as the material response of lunar or asteroidal rocks might be sizably different to that of terrestrial counterparts, making simulant materials non-reliable to test processes and materials for future lunar surface engineering construction.

While promising and informative, the present HP-XRD results are still limited due to the relatively large errors in the fitted EoS parameters. In spite of this, it is clear that HP-XRD experiments offer a promising avenue for future investigations into the elastic properties of meteorite minerals. For instance, HP-XRD measurements on individual chondrules or mineral grains could provide clear evidence of modified compression properties of meteorite minerals. Other techniques, like Raman scattering measurements, could provide complementary information without the need of synchrotron-based experiments. Finally, HP experiments on samples that have undergone thermal or shock-wave treatments, or space weathering (e.g., proton bombardment), could be highly informative in order to understand the role

of such processes on the mechanical and elastic properties of planetary minerals at the chemical bond scale.

4. Conclusions

In this work, we have analyzed the mechanical and high-pressure structural properties of olivine in the NWA 12008 lunaite and some chondritic meteorites. Olivine has long been studied for its relevance in Earth sciences and, in particular, for its high abundance in Earth's mantle. In the context of extraterrestrial geochemistry, olivine is also present in high proportions in many planetary bodies, and therefore its study is relevant, among others, for ISRU or for planetary defense.

We determined the hardness and reduced elastic modulus of numerous olivine grains of the NWA 12008 meteorite using the nanoindentation technique. For completeness, we performed similar experiments on a control terrestrial olivine sample. Our results suggest that the lunar olivine is softer and more elastic by a 31% and a 26%, respectively, compared with terrestrial olivine. Individual nanoindentations of terrestrial and lunar olivines show two different distributions of hardness and reduced elastic modulus. The observed softening might be attributed to macroscale phenomena, like porosity or microfracturing, or to changes at the level of the crystal lattice.

On the other hand, we performed HP-XRD measurements to investigate the compressibility behavior of olivine in NWA 12008. For comparison purposes, we also performed HP-XRD measurements on three different ordinary chondrites. These experiments suggest that olivine, or at least its b orthorhombic axis, might be more compressible in NWA 12008 and in some chondrites relative to terrestrial olivine. This would support the results of the nanoindentation experiments and confirm that, at least in part, the softening observed with the nanoindentations might be related to structural changes at the chemical bond scale.

The possibility that the observed differences might be due solely to a compositional effect can mostly be ruled out, as no clear trend is seen in the results of the nanoindentations when considering the %Fo content of the analysed olivine grains. The HP-XRD results suggest that olivine in NWA 12008 and in some of the studied chondrites is different, at a structural level, than the terrestrial counterpart. For instance, lattice disorder induced by shock metamorphism or space weathering might have affected the mechanical and elastic behavior of the mineral.

The fact that lunar and asteroidal olivines exhibit modified mechanical behavior compared to terrestrial olivine is of great relevance both from a fundamental point of view but also for ISRU applications and future space missions. Overall, this work confirms previous results (Peña-Asensio et al., 2024; Moyano-Camero et al., 2017) suggesting that the mechanical properties of some mineral constituents of planetary materials might be different than those on Earth. Nevertheless, more work is still required in order to unambiguously confirm the present conclusions. In particular,

more nanoindentations should be conducted over a larger number of olivines on other extraterrestrial bodies to confirm these findings. It would be particularly interesting to measure the mechanical properties of olivine in a returned sample, other than a meteorite. With such experiments, for instance, the possible role of shock metamorphism on the properties of meteoritic materials could be discarded.

In conclusion, the combination of nanoindentations and HP-XRD measurements to investigate the mechanical and elasticity properties of extraterrestrial minerals offers a promising avenue for future research in planetary science and may become a widely adopted methodology to characterize planetary materials. New HP-XRD experiments ought to be performed in order to better constrain the EoS parameters of lunar and asteroidal olivine, as well as of that of other minerals from meteorites and returned samples.

Acknowledgements

Financial support from the project PID2021-128062NB-I00 funded by the Spanish Ministerio de Ciencia, Innovación y Universidades MCIU (DOI:10.13039/501100011033) is acknowledged, as well as the Spanish program Unidad de Excelencia María de Maeztu CEX2020-001058-M. The ALBA-CELLS synchrotron is acknowledged for granting beamtime at the MSPD beamline under projects 2021095390 and 2022025734. PG-T acknowledges the financial support from the Spanish MCIU through the FPI predoctoral fellowship PRE2022-104624. JS acknowledges the financial support from projects 2021-SGR-00651 and PID2020-116844RB-C21. EP-A acknowledges financial support from the LUMIO project funded by the Agenzia Spaziale Italiana (2024-6-HH.0). DE thanks the financial support from Spanish MCIU under projects PID2022-138076NB-C41 and RED2022-134388-T and from Generalitat Valenciana (GVA) through grants CIPROM/2021/075 and MFA/2022/007, which is part of the Advanced Materials program and is supported with funding from the European Union Next Generation EU (PRTR-C17.11). RT and DE (PB and DE) thank GVA for the Postdoctoral Fellowship CIAPOS/2021/20 (CIAPOS/2023/406). JS-M thanks the Spanish MCIU for the PRE2020-092198 fellowship. The authors also acknowledge financial support from PID2020-116844RB-C21 and 2021-SGR-00651. NWA 12008 has been studied within the framework of an international European consortium led by IFP. Special acknowledge to I. Weber for providing the NWA 12008 meteorite thin section. This work is part of the doctoral thesis of PG-T (Doctoral Program in Physics at Universitat Autònoma de Barcelona).

References

- Angel, R., Mazzucchelli, M., Alvaro, M., Nimis, P., Nestola, F., 2014. Letter: geobarometry from host-inclusion systems: The role of elastic relaxation. *American Mineralogist* 99, 2146–2149. doi:10.2138/am-2014-5047.
- Angel, R., Nimis, P., Mazzucchelli, M., Alvaro, M., Nestola, F., 2015. How large are departures from lithostatic pressure? constraints from host-inclusion elasticity. *Journal of Metamorphic Geology* 33. doi:10.1111/jmg.12138.
- Angel, R.J., 2000. Equations of state. *Reviews in Mineralogy and Geochemistry* 41, 35–59. doi:10.2138/rmg.2000.41.2.
- Avadani, D., Hansen, L., Marquardt, K., Wallis, D., Ohl, M., Wilkinson, A., 2023. The Role of Grain Boundaries in Low-Temperature Plasticity of Olivine Revealed by Nanoindentation. *Journal of Geophysical Research (Solid Earth)* 128, e2023JB026763. doi:10.1029/2023JB026763.
- Ayatollahi, M.R., Najafabadi, M., R. Kolor, S., Petru, M., 2020. Mechanical characterization of heterogeneous polycrystalline rocks using nanoindentation method in combination with generalized means method. *Journal of Mechanics* 36, 1–11. doi:10.1017/jmech.2020.18.
- Badt, N., Goldsby, D.L., 2023. Attenuation of olivine single crystals using nanoindentation, in: AGU Fall Meeting Abstracts, pp. MR31A–0045.
- Baral, P., Orekhov, A., Dohmen, R., Coulombier, M., Raskin, J.P., Cordier, P., Idrissi, H., Pardo, T., 2021. *Acta Materialia* 219, 117257. doi:https://doi.org/10.1016/j.actamat.2021.117257.
- Bass, J.D., 1995. Elasticity of Minerals, Glasses, and Melts. *American Geophysical Union (AGU)*. pp. 45–63. doi:https://doi.org/10.1029/RF002p0045.
- Biener, J., Hodge, A.M., Hamza, A.V., Hsiung, L.M., Satcher, Joe H., J., 2004. Nanoporous au: A high yield strength material. *Journal of Applied Physics* 97, 024301. doi:10.1063/1.1832742.
- Brantley, S.L., Mellott, N.P., 2000. Surface area and porosity of primary silicate minerals. *American Mineralogist* 85, 1767–1783. doi:10.2138/am-2000-11-1220.
- Cariou, S., Ulm, F.J., Dormieux, L., 2008. Hardness–packing density scaling relations for cohesive–frictional porous materials. *Journal of the Mechanics and Physics of Solids* 56, 924–952. doi:https://doi.org/10.1016/j.jmps.2007.06.011.
- Chandra, U., Pandey, K., Parthasarathy, G., Sharma, S.M., 2016. High-pressure investigations on pliaia kalan eucrite meteorite using in-situ x-ray diffraction and 57Fe Mössbauer spectroscopic technique up to 16 gpa. *Geoscience Frontiers* 7, 265–271. doi:https://doi.org/10.1016/j.gsf.2015.05.003. special Issue: Exhuming Asia.
- Chandra, U., Parthasarathy, G., Chandra Shekar, N.V., Sahu, P., 2013. X-ray diffraction, Mössbauer spectroscopic and electrical resistivity studies on lohawat meteorite under high-pressure up to 9 gpa. *Chemie der Erde* 73, 197–203.
- Chen, X.Q., Niu, H., Li, D., Li, Y., 2011. Modeling hardness of polycrystalline materials and bulk metallic glasses. *Intermetallics* 19, 1275–1281. doi:https://doi.org/10.1016/j.intermet.2011.03.026.
- Cheng, A.F., Agrusa, H.F., Barbee, B.W., Meyer, A.J., Farnham, T.L., Raducan, S.D., Richardson, D.C., Dotto, E., Zinzi, A., Della Corte, V., Statler, T.S., Chesley, S., Naidu, S.P., Hirabayashi, M., Li, J.Y., Egl, S., Barnouin, O.S., Chabot, N.L., Chocron, S., Collins, G.S., Daly, R.T., Davison, T.M., DeCoster, M.E., Ernst, C.M., Ferrari, F., Graninger, D.M., Jacobson, S.A., Jutzi, M., Kumamoto, K.M., Luther, R., Lyzhoft, J.R., Michel, P., Murdoch, N., Nakano, R., Palmer, E., Rivkin, A.S., Scheeres, D.J., Stickle, A.M., Sunshine, J.M., Trigo-Rodríguez, J.M., Vincent, J.B., Walker, J.D., Wünnemann, K., Zhang, Y., Amoroso, M., Bertini, I., Brucato, J.R., Capannolo, A., Cremonese, G., Dall’Ora, M., Deshpriya, P.J.D., Gai, I., Hasselmann, P.H., Ieva, S., Impresario, G., Ivanovski, S.L., Lavagna, M., Lucchetti, A., Epifani, E.M., Modenini, D., Pajola, M., Palumbo, P., Perna, D., Pirrotta, S., Poggiali, G., Rossi, A., Tortora, P., Zannoni, M., Zanotti, G., 2023. *Nature* 616, 457–460.
- Chudoba, T., Schwaller, P., Rabe, R., Breguet, J.M., Michler, J., 2006. Comparison of nanoindentation results obtained with berkovich and cube-corner indenters. *Philosophical Magazine* 86, 5265–5283. doi:10.1080/14786430600746424.
- Daly, R.T., Ernst, C.M., Barnouin, O.S., Chabot, N.L., Rivkin, A.S., Cheng, A.F., Adams, E.Y., Agrusa, H.F., Abel, E.D., Alfoud, A.L., Asphaug, E.I., Atchison, J.A., Badger, A.R., Baki, P., Ballouz, R.L., Bekker, D.L., Bellerose, J., Bhaskaran, S., Buratti, B.J., Cambioni, S., Chen, M.H., Chesley, S.R., Chiu, G., Collins, G.S., Cox, M.W., DeCoster, M.E., Ericksen, P.S., Espiritu, R.C., Faber, A.S., Farnham, T.L., Ferrari, F., Fletcher, Z.J., Gaskell, R.W., Graninger, D.M., Haque, M.A., Harrington-Duff, P.A., Hefter, S., Herreros, I., Hirabayashi, M., Huang, P.M., Hsieh, S.Y.W., Jacobson, S.A., Jenkins, S.N., Jensenius, M.A., John, J.W., Jutzi, M., Kohout, T., Krueger, T.O., Laipert, F.E., Lopez,

- N.R., Luther, R., Lucchetti, A., Mages, D.M., Marchi, S., Martin, A.C., McQuaide, M.E., Michel, P., Moskovitz, N.A., Murphy, I.W., Murdoch, N., Naidu, S.P., Nair, H., Nolan, M.C., Ormó, J., Pajola, M., Palmer, E.E., Peachey, J.M., Pravec, P., Raducan, S.D., Ramesh, K.T., Ramirez, J.R., Reynolds, E.L., Richman, J.E., Robin, C.Q., Rodriguez, L.M., Roufberg, L.M., Rush, B.P., Sawyer, C.A., Scheeres, D.J., Scheirich, P., Schwartz, S.R., Shannon, M.P., Shapiro, B.N., Shearer, C.E., Smith, E.J., Steele, R.J., Steckloff, J.K., Stickle, A.M., Sunshine, J.M., Superfin, E.A., Tarzi, Z.B., Thomas, C.A., Thomas, J.R., Trigo-Rodríguez, J.M., Trops, B.T., Vaughan, A.T., Velez, D., Waller, C.D., Wilson, D.S., Wortman, K.A., Zhang, Y., 2023. Successful kinetic impact into an asteroid for planetary defence. *Nature* 616, 443–447. doi:10.1038/s41586-023-05810-5.
- Davison, T.M., Collins, G.S., Bland, P.A., 2016. Mesoscale Modelling of Impact Compaction of Primitive Solar System Solids, in: LPI Editorial Board (Ed.), 79th Annual Meeting of the Meteoritical Society, p. 6395.
- Demouchy, S., 2021. Defects in olivine. *European Journal of Mineralogy* 33, 249–282. doi:10.5194/ejm-33-249-2021.
- Dewaele, A., Loubeyre, P., Mezouar, M., 2004. Equations of state of six metals above 94 GPa. *Phys. Rev. B* 70, 094112. doi:10.1103/PhysRevB.70.094112.
- Duffard, R.D., Gómez, I.G., Jurado, M.J., Trigo-Rodríguez, J.M., Rossi, C., Schimmel, M., Zorzano, M.P., 2021. CHALLENGE 1: IN-SITU RESOURCES UTILIZATION. Technical Report. Consejo Superior de Investigaciones Científicas (CSIC). doi:10.20350/digitalCSIC/12659.
- Durga Prasad, K., Bhatt, M., A., Ambily, G., Sathyan, S., Misra, D., Srivastava, N., Bhardwaj, A., 2023. Contextual characterization study of Chandrayaan-3 primary landing site. *Monthly Notices of the Royal Astronomical Society: Letters* 526, L116–L123. doi:10.1093/mnrasl/slad106.
- Fauth, F., Peral, I., Popescu, C., Knapp, M., 2013. The new material science powder diffraction beamline at alba synchrotron. *Powder Diffraction* 28, S360–S370. doi:10.1017/S0885715613000900.
- Fegley, Jr., B., 2003. Venus. *Treatise on Geochemistry* 1, 711. doi:10.1016/B0-08-043751-6/01150-6.
- Fischer-Cripps, A., Nicholson, D., 2004. Nanindentation. *Mechanical Engineering Series. Applied Mechanics Reviews* 57, B12. doi:10.1115/1.1704625.
- Gattacceca, J., McCubbin, F.M., Bouvier, A., Grossman, J., 2020. The Meteoritical Bulletin, No. 107. *MAPS* 55, 460–462.
- Gholami, S., Zhang, X., Kim, Y.J., Kim, Y.R., Cui, B., Shin, H.S., Lee, J., 2022. Hybrid microwave sintering of a lunar soil simulant: Effects of processing parameters on microstructure characteristics and mechanical properties. *Materials & Design* 220, 110878. doi:https://doi.org/10.1016/j.matdes.2022.110878.
- Gonzalez-Platas, J., Alvaro, M., Nestola, F., Angel, R., 2016. *EosFit7-GUI*: a new graphical user interface for equation of state calculations, analyses and teaching. *Journal of Applied Crystallography* 49, 1377–1382. doi:10.1107/S1600576716008050.
- Hoover, C.G., Jardine, K.J., Ryan, A.J., Sanchez, P., Biele, J., Ballouz, R.L., Macke, R.J., Landsman, Z.A., Long-Fox, J.M., Connolly, H.C., Lauretta, D.S., 2024. Bennu Sample Physical Properties from Multi-Scale Measurements of Strength and Indentation Hardness, in: LPI Contributions, p. 2480.
- Horii, Youichi, Fujii, Naoyuki, Takeda, Hiroshi, 1990. Hardness analysis of metallic particles in ordinary chondrites, in: Proceedings of the NIPR Symposium, National Institute of Polar Research. p. 254.
- Jha, K.K., Suksawang, N., Lahiri, D., Agarwal, A., 2012. Energy-based analysis of nanoindentation curves for cementitious materials. *Materials* 109, 81–90. doi:10.14359/5168573.
- Jiang, Q., ichiro Karato, S., Datye, A., Yang, S., Foteinou, V., Rogalla, D., Schwarz, U.D., 2024. Weakening of olivine by hydrogen implantation: Results of nano-indentation tests and some applications to planetary materials. *Icarus* 421, 116243. doi:https://doi.org/10.1016/j.icarus.2024.116243.
- Jones, A., 2000. Depletion patterns and dust evolution in the interstellar medium. *Journal of Geophysical Research* 105. doi:10.1029/1999JA900264.
- Kranjc, K., Rouse, Z., Flores, K.M., Skemer, P., 2016. Low-temperature plastic rheology of olivine determined by nanoindentation. *Geophysical Research Letters* 43, 176–184. doi:https://doi.org/10.1002/2015GL065837.
- Kranjc, K., Thind, A.S., Borisevich, A.Y., Mishra, R., Flores, K.M., Skemer, P., 2020. Amorphization and plasticity of olivine during low-temperature micropillar deformation experiments. *Journal of Geophysical Research: Solid Earth* 125, e2019JB019242. doi:https://doi.org/10.1029/2019JB019242. e2019JB019242 2019JB019242.
- Kumamoto, K.M., Hansen, L.N., Breithaupt, T., Wallis, D., Li, B.S., Armstrong, D.E.J., Goldsby, D.L., Li, Y.W., Warren, J.M., Wilkinson, A.J., 2024. The effect of intracrystalline water on the mechanical properties of olivine at room temperature. *Geophysical Research Letters* 51, e2023GL106325. doi:https://doi.org/10.1029/2023GL106325. e2023GL106325 2023GL106325.
- Lauretta, D.S., Balram-Knutson, S.S., Beshore, E., Boynton, W.V., Drouet d'Aubigny, C., DellaGiustina, D.N., Enos, H.L., Golish, D.R., Hergenrother, C.W., Howell, E.S., Bennett, C.A., Morton, E.T., Nolan, M.C., Rizk, B., Roper, H.L., Bartels, A.E., Bos, B.J., Dworkin, J.P., Highsmith, D.E., Lorenz, D.A., Lim, L.F., Mink, R., Moreau, M.C., Nuth, J.A., Reuter, D.C., Simon, A.A., Bierhaus, E.B., Bryan, B.H., Ballouz, R., Barnouin, O.S., Binzel, R.P., Bottke, W.F., Hamilton, V.E., Walsh, K.J., Chesley, S.R., Christensen, P.R., Clark, B.E., Connolly, H.C., Crombie, M.K., Daly, M.G., Emery, J.P., McCoy, T.J., McMahon, J.W., Scheeres, D.J., Messenger, S., Nakamura-Messenger, K., Righter, K., Sandford, S.A., 2017. Osiris-rex: Sample return from asteroid (101955) bennu. *Space Science Reviews* 212, 925–984. doi:10.1007/s11214-017-0405-1.
- Lim, S., Prabhu, V.L., Anand, M., Taylor, L.A., 2017. Extra-terrestrial construction processes – advancements, opportunities and challenges. *Advances in Space Research* 60, 1413–1429. doi:https://doi.org/10.1016/j.asr.2017.06.038.
- Lin, T.D., Love, H., Stark, D., 1988. Physical Properties of Concrete Made with Apollo 16 Lunar Soil Sample, in: LPI Editorial Board (Ed.), Second Conference on Lunar Bases and Space Activities of the 21st Century, p. 159.
- Liu, B., Sun, P., Yao, W., Li, T., Xu, W., 2024. Research progress on the adaptability of lunar regolith simulant-based composites and lunar base construction methods. *International Journal of Mining Science and Technology* 34, 1341–1363. doi:https://doi.org/10.1016/j.ijmst.2024.09.005.
- Liu, K., Ostadhassan, M., Bubach, B., 2016. Applications of nano-indentation methods to estimate nanoscale mechanical properties of shale reservoir rocks. *Journal of Natural Gas Science and Engineering* 35, 1310–1319. doi:https://doi.org/10.1016/j.jngse.2016.09.068.
- Ma, Z., Gamage, R.P., Zhang, C., 2020. Application of nanoindentation technology in rocks: a review. *Geomechanics and Geophysics for Geo-Energy and Geo-Resources* 6, 60. doi:10.1007/s40948-020-00178-6.
- Macke, R.J., Britt, D.T., Consolmagno, G.J., 2011. Density, porosity, and magnetic susceptibility of achondritic meteorites. *Meteoritics & Planetary Science* 46, 311–326. doi:https://doi.org/10.1111/j.1945-5100.2010.01155.x.
- Macke, R.J., Consolmagno, G.J., Britt, D.T., Hutson, M.L., 2010. Enstatite chondrite density, magnetic susceptibility, and porosity. *MAPS* 45, 1513–1526. doi:10.1111/j.1945-5100.2010.01129.x.
- MacKenzie, W., Adams, A., 1994. A Colour Atlas of Rocks and Minerals in Thin Section. *Manson Series*, Manson.
- Mackwell, S.J., Bai, Q., Kohlstedt, D.L., 1990. Rheology of olivine and the strength of the lithosphere. *Geophysical Research Letters* 17, 9–12. doi:https://doi.org/10.1029/GL017i001p00009.
- Magoarić, H., Danescu, A., 2009. Modeling macroscopic elasticity of porous silicon. *physica status solidi c* 6, 1680–1684. doi:https://doi.org/10.1002/pssc.200881053.
- Mazzucchelli, M., Reali, A., Morganti, S., Angel, R., Alvaro, M., 2019. Elastic geobarometry for anisotropic inclusions in cubic hosts. *Lithos* 350-351, 105218. doi:https://doi.org/10.1016/j.lithos.2019.105218.
- Min, M., Waters, L. B. F. M., de Koter, A., Hovenier, J. W., Keller, L. P., Markwick-Kemper, F., 2007. The shape and composition of interstellar

- silicate grains. *A&A* 462, 667–676. URL: <https://doi.org/10.1051/0004-6361:20065436>, doi:10.1051/0004-6361:20065436.
- Morgan, J.W., Anders, E., 1980. Chemical Composition of Earth, Venus, and Mercury. *Proceedings of the National Academy of Science* 77, 6973–6977. doi:10.1073/pnas.77.12.6973.
- Moyano-Camero, C.E., Pellicer, E., Trigo-Rodríguez, J.M., Williams, I.P., Blum, J., Michel, P., Küppers, M., Martínez-Jiménez, M., Lloro, I., Sort, J., 2017. *ApJ* 835, 157.
- NASA, 2020. NASA's Plan for Sustained Lunar Exploration and Development. Technical Report. NASA.
- Naser, M., 2019. Extraterrestrial construction materials. *Progress in Materials Science* 105, 100577. doi:<https://doi.org/10.1016/j.pmatsci.2019.100577>.
- Nestola, F., Pasqual, D., Smyth, J., Novella, D., Secco, L., Manghni, M., Negro, A.D., 2011. New accurate elastic parameters for the forsterite-fayalite solid solution. *American Mineralogist* 96, 1742–1747. doi:10.2138/am.2011.3829.
- Neves, J.M., Ramanathan, S., Suraneni, P., Grugel, R., Radlińska, A., 2020. Characterization, mechanical properties, and microstructural development of lunar regolith simulant-portland cement blended mixtures. *Construction and Building Materials* 258, 120315. doi:<https://doi.org/10.1016/j.conbuildmat.2020.120315>.
- Nie, J., Cui, Y., Senetakis, K., Guo, D., Wang, Y., Wang, G., Feng, P., He, H., Zhang, X., Zhang, X., Li, C., Zheng, H., Hu, W., Niu, F., Liu, Q., Li, A., 2023. Predicting residual friction angle of lunar regolith based on chang'e-5 lunar samples. *Science Bulletin* 68, 730–739. doi:<https://doi.org/10.1016/j.scib.2023.03.019>.
- Oliver, W.C., Pharr, G.M., 1992. An improved technique for determining hardness and elastic modulus using load and displacement sensing indentation experiments. *Journal of Materials Research* 7, 1564–1583. doi:10.1557/JMR.1992.1564.
- Oliver, W.C., Pharr, G.M., 2011. Nanoindentation in materials research: Past, present, and future. *MRS Bulletin* 35, 897–907. doi:10.1557/mrs2010.717.
- Peña-Asensio, E., Trigo, Rodríguez, J.M., Sort, J., Ibáñez-Insa, J., Rimola, A., 2024. Mechanical Properties of Minerals in Lunar and HED Meteorites from Nanoindentation Testing: Implications for Space Mining. *arXiv e-prints* doi:10.48550/arXiv.2402.03960.
- Pellicer, E., Pané, S., Panagiotopoulou, V., Fusco, S., Sivaraman, K., Suriñach, S., Baró, M., Nelson, B., Sort, J., 2012. Localized electrochemical deposition of porous Cu-Ni microcolumns: Insights into the growth mechanisms and the mechanical performance. *International Journal of Electrochemical Science* 7, 4014–4029. doi:10.1016/S1452-3981(23)19516-2.
- Peslier, A., Woodland, A., Bell, D., 2010. Olivine water contents in the continental lithosphere and the longevity of cratons. *Nature* 467, 78–81. doi:<https://doi.org/10.1038/nature09317>.
- Peña-Asensio, E., Trigo-Rodríguez, J.M., Sort, J., Ibáñez-Insa, J., Rimola, A., 2024. Machine learning applications on lunar meteorite minerals: From classification to mechanical properties prediction. *International Journal of Mining Science and Technology* 34, 1283–1292. doi:<https://doi.org/10.1016/j.ijmst.2024.08.001>. *planetary Rock and Soil Mechanics*.
- Pilehvar, S., Arnhof, M., Pamies, R., Valentini, L., Kjøniksen, A.L., 2020. Utilization of urea as an accessible superplasticizer on the moon for lunar geopolymer mixtures. *Journal of Cleaner Production* 247, 119177. doi:<https://doi.org/10.1016/j.jclepro.2019.119177>.
- Prescher, C., Prakapenka, V.B., 2015. DIOPTAS: a program for reduction of two-dimensional X-ray diffraction data and data exploration. *High Pressure Research* 35, 223–230. doi:10.1080/08957959.2015.1059835.
- Raducan, S.D., Jutzi, M., Cheng, A.F., Zhang, Y., Barnouin, O., Collins, G.S., Daly, R.T., Davison, T.M., Ernst, C.M., Farnham, T.L., Ferrari, F., Hirabayashi, M., Kumamoto, K.M., Michel, P., Murdoch, N., Nakano, R., Pajola, M., Rossi, A., Agrusa, H.F., Barbee, B.W., Syal, M.B., Chabot, N.L., Dotto, E., Fahnestock, E.G., Hasselmann, P.H., Herreros, I., Ivanovski, S., Li, J.Y., Lucchetti, A., Luther, R., Ormó, J., Owen, M., Pravec, P., Rivkin, A.S., Robin, C.Q., Sánchez, P., Tusberti, F., Wünnemann, K., Zinzi, A., Epifani, E.M., Manzoni, C., May, B.H., 2024. Physical properties of asteroid dimorphos as derived from the dart impact. *Nature Astronomy* 8, 445–455. doi:10.1038/s41550-024-02200-3.
- Ramakrishnan, N., Arunachalam, V.S., 1993. Effective elastic moduli of porous ceramic materials. *Journal of the American Ceramic Society* 76, 2745–2752. doi:<https://doi.org/10.1111/j.1151-2916.1993.tb04011.x>.
- Robin, C.Q., Duchene, A., Murdoch, N., Vincent, J.B., Lucchetti, A., Pajola, M., Ernst, C.M., Daly, R.T., Barnouin, O.S., Raducan, S.D., Michel, P., Hirabayashi, M., Stott, A., Cuervo, G., Jawin, E.R., Trigo-Rodríguez, J.M., Parro, L.M., Sunday, C., Vivet, D., Mimoun, D., Rivkin, A.S., Chabot, N.L., 2024. Mechanical properties of rubble pile asteroids (dimorphos, itokawa, ryugu, and bennu) through surface boulder morphological analysis. *Nature Communications* 15, 6203. doi:10.1038/s41467-024-50147-w.
- Ronco, M.P., Thiabaud, A., Marboeuf, U., Alibert, Y., de Elfa, G.C., Guilera, O.M., 2015. Chemical composition of Earth-like planets. *Boletín de la Asociación Argentina de Astronomía La Plata Argentina* 57, 251–253. doi:10.48550/arXiv.1502.06870.
- Roth, N.X., Milam, S.N., Remijan, A.J., Cordiner, M.A., Busch, M.W., Thomas, C.A., Rivkin, A.S., Moullet, A., Roush, T.L., Siebert, M.A., Li, J.Y., Fahnestock, E.G., Trigo-Rodríguez, J.M., Opitom, C., Hirabayashi, M., 2023. Alma observations of the dart impact: Characterizing the ejecta at submillimeter wavelengths. *The Planetary Science Journal* 4, 206. doi:10.3847/PSJ/acfcaa.
- Rubin, A.E., Ma, C., 2017. Meteoritic minerals and their origins. *Chemie der Erde* , 325–385doi:10.1016/j.chemer.2017.01.005.
- Tabor, D., 2000. *The Hardness of Metals. Monographs on the physics and chemistry of materials*, OUP Oxford.
- Tanbakouei, S., Trigo-Rodríguez, J.M., Sort, J., Michel, P., Blum, J., Nakamura, T., Williams, I., 2019. *AAP* 629, A119.
- Tang, X., Xu, J., Zhang, Y., Zhao, H., Paluszny, A., Wan, X., Wang, Z., 2023. The rock-forming minerals and macroscale mechanical properties of asteroid rocks. *Engineering Geology* 321, 107154. doi:<https://doi.org/10.1016/j.enggeo.2023.107154>.
- Tardivel, S., Scheeres, D.J., Michel, P., Van wal, S., Sánchez, P., 2014. Contact Motion on Surface of Asteroid. *Journal of Spacecraft and Rockets* 51, 1857–1871. doi:10.2514/1.A32939.
- Taylor, G.J., Scott, E.R.D., 2003. *Mercury. Treatise on Geochemistry* 1, 711. doi:10.1016/B00-08-043751-6/01071-9.
- Thomas, C.A., Naidu, S.P., Scheirich, P., Moskovitz, N.A., Pravec, P., Chesley, S.R., Rivkin, A.S., Osip, D.J., Lister, T.A., Benner, L.A.M., Brozović, M., Contreras, C., Morrell, N., Rožek, A., Kušnirák, P., Hornoch, K., Mages, D., Taylor, P.A., Seymour, A.D., Snodgrass, C., Jørgensen, U.G., Dominik, M., Skiff, B., Polakis, T., Knight, M.M., Farnham, T.L., Giorgini, J.D., Rush, B., Bellerose, J., Salas, P., Armentrout, W.P., Watts, G., Busch, M.W., Chatelain, J., Gomez, E., Greenstreet, S., Phillips, L., Bonavita, M., Burgdorf, M.J., Khalouei, E., Longa-Peña, P., Rabus, M., Sajadian, S., Chabot, N.L., Cheng, A.F., Ryan, W.H., Ryan, E.V., Holt, C.E., Agrusa, H.F., 2023. Orbital period change of dimorphos due to the dart kinetic impact. *Nature* 616, 448–451. doi:10.1038/s41586-023-05805-2.
- Tolu, E., Garroni, S., Pellicer, E., Sort, J., Milanese, C., Cosseddu, P., Enzo, S., Baró, M., Mulas, G., 2013. Highly ordered mesoporous magnesium niobate high- κ dielectric ceramic: Synthesis, structural/mechanical characterization and thermal stability. *J. Mater. Chem. C* 1. doi:10.1039/C3TC30500G.
- Wang, C., Jia, Y., Xue, C., Lin, Y., Liu, J., Fu, X., Xu, L., Huang, Y., Zhao, Y., Xu, Y., Gao, R., Wei, Y., Tang, Y., Yu, D., Zou, Y., 2023. Scientific objectives and payload configuration of the chang'e-7 mission. *National Science Review* 11, nwad329. doi:10.1093/nsr/nwad329.
- Watanabe, S., Hirabayashi, M., Hirata, N., Hirata, N., Noguchi, R., Shimaki, Y., Ikeda, H., Tatsumi, E., Yoshikawa, M., Kikuchi, S., Yabuta, H., Nakamura, T., Tachibana, S., Ishihara, Y., Morota, T., Kitazato, K., Sakatani, N., Matsumoto, K., Wada, K., Senshu, H., Honda, C., Michikami, T., Takeuchi, H., Kouyama, T., Honda, R., Kameda, S., Fuse, T., Miyamoto, H., Komatsu, G., Sugita, S., Okada, T., Namiki, N., Arakawa, M., Ishiguro, M., Abe, M., Gaskell, R., Palmer, E., Barnouin,

- O.S., Michel, P., French, A.S., McMahon, J.W., Scheeres, D.J., Abell, P.A., Yamamoto, Y., Tanaka, S., Shirai, K., Matsuoka, M., Yamada, M., Yokota, Y., Suzuki, H., Yoshioka, K., Cho, Y., Tanaka, S., Nishikawa, N., Sugiyama, T., Kikuchi, H., Hemmi, R., Yamaguchi, T., Ogawa, N., Ono, G., Mimasu, Y., Yoshikawa, K., Takahashi, T., Takei, Y., Fujii, A., Hirose, C., Iwata, T., Hayakawa, M., Hosoda, S., Mori, O., Sawada, H., Shimada, T., Soldini, S., Yano, H., Tsukizaki, R., Ozaki, M., Iijima, Y., Ogawa, K., Fujimoto, M., Ho, T.M., Moussi, A., Jaumann, R., Bibring, J.P., Krause, C., Terui, F., Saiki, T., Nakazawa, S., Tsuda, Y., 2019. Hayabusa2 arrives at the carbonaceous asteroid 162173 Ryugu—A spinning top-shaped rubble pile. *Science* 364, 268–272. doi:10.1126/science.aav8032.
- Xu, J.J., Zhang, Y.H., Rutqvist, J., Hu, M.S., Wang, Z.Z., Tang, X.H., 2023. Thermally Induced Microcracks in Granite and Their Effect on the Macroscale Mechanical Behavior. *Journal of Geophysical Research (Solid Earth)* 128, e2022JB024920. doi:10.1029/2022JB024920.
- Yano, H., Kubota, T., Miyamoto, H., Okada, T., Scheeres, D., Takagi, Y., Yoshida, K., Abe, M., Abe, S., Barnouin-Jha, O., Fujiwara, A., Hasegawa, S., Hashimoto, T., Ishiguro, M., Kato, M., Kawaguchi, J., Mukai, T., Saito, J., Sasaki, S., Yoshikawa, M., 2006. Touchdown of the Hayabusa Spacecraft at the Muses Sea on Itokawa. *Science* 312, 1350–1353. doi:10.1126/science.1126164.
- Yomogida, K., Matsui, T., 1983. Physical properties of ordinary chondrites and their implications. *Meteoritics* 18, 430–431.
- Zhang, L., 1998. Single crystal hydrostatic compression of (mg,mn,fe,co)₂siO₄ olivines. *Physics and Chemistry of Minerals* 25, 308–312.